ACS Catalysis

Article

Eco-Friendly Photochemical Production of H2O2 through O2 Reduction over Carbon Nitride Frameworks Incorporated with Multiple Hetero-Elements

Gun-hee Moon, Mamoru Fujitsuka, Sooyeon Kim, Tetsuro Majima, Xinchen Wang, and Wonyong Choi

ACS Catal., **Just Accepted Manuscript** • DOI: 10.1021/acscatal.6b03334 • Publication Date (Web): 13 Mar 2017

Eco-Friendly Photochemical Production of H_2O_2 through O_2 Reduction over Carbon Nitride Frameworks Incorporated with Multiple Hetero-Elements

Gun-hee Moon[1], Mamoru Fujitsuka[2], Sooyeon Kim[2], Tetsuro Majima[2], Xinchen Wang[3], and Wonyong Choi[1]*

[1] Department of Chemical Engineering & Division of Environmental Science and Engineering, Pohang University of Science and Technology (POSTECH), Pohang, 37673 Korea

[2] The Institute of Scientific and Industrial Research (SANKEN), Osaka University, Osaka 567-0047, Japan

[3] College of Chemistry, Fuzhou University, Fuzhou 350002, P. R. China

Submitted to

ACS Catalysis

* To whom correspondence should be addressed (W. Choi)

E-mail: wchoi@postech.edu Fax: +82-54-279-8299

Abstract

We report that in-situ incorporation of both potassium and phosphate species into polymeric carbon nitride (CN) framework highly enhanced the photo-production of hydrogen peroxide (H_2O_2) without the use of any noble metal co-catalysts. The incorporation of the earth-abundant hetero-elements (K, P, and O) (i) introduced the negative surface charge over the entire pH through the surface functionalization by phosphate species, (ii) increased the lifetime of the transient species in picosecond timescale via the formation of charge separation states, (iii) facilitated the interfacial electron transfer to dioxygen, and (iv) inhibited the decomposition of in-situ generated H_2O_2. As a result, the modified CN showed the apparent quantum yields (Φ: for H_2O_2 production) that are enhanced by about 25 and 17 times (Φ_{420} = 8.0%; Φ_{320} = 26.2%) from those of bare CN (Φ_{420} = 0.32%; Φ_{320} = 1.55%) under monochromatic irradiation of 420 and 320 nm, respectively. This study clearly demonstrated a simple way to design multiple hetero-elements incorporated CN compounds that consist of earth-abundant elements only (C, N, K, P, O) for the development of practical and economical solar conversion photocatalytic materials.

Keywords: Photocatalysis, Carbon nitride, Solar fuel, Hydrogen peroxide synthesis, Proton coupled electron transfer (PCET)

1. Introduction

The practical application of photocatalysts associated with metal oxide/sulfide/nitride should overcome many critical problems including a low solar light absorption, a low conversion/selectivity, a lack of long-term stability, a high operating cost, etc.[1,2] In this regard, polymeric carbon nitride consisting of earth-abundant carbon and nitrogen elements only is an attractive material because of its visible light absorption capability and the superior stability against photo-corrosion. Furthermore, the conduction band (CB) and valence band (VB) potentials (E_{CB} = -1.3 V_{NHE} and E_{VB} = 1.4 V_{NHE} at pH 7) are thermodynamically suitable for various reactions such as water-splitting, partial oxidation, oxygen reduction reaction (ORR), and the degradation of organic pollutants.[3] On the other hand, a still low photo-conversion efficiency needs to be overcome, so various strategies such as morphology control, doping, bandgap engineering, co-catalysts loading, and hybridization with other materials have been actively investigated.[4]

Hydrogen peroxide (H_2O_2) is an eco-friendly oxidant that is widely utilized for chemical synthesis, disinfection, bleaching agent, liquid propellant, Fenton reaction, etc. H_2O_2 can be produced by the reaction of H_2 and O_2 via anthraquinone method[5] or the reduction of O_2 through proton-coupled electron transfer (PCET) ($O_2 + 2H^+ + 2e^- \rightarrow H_2O_2$; E^0 = 0.695 V_{NHE}).[6] The photosynthetic production of H_2O_2 through PCET is safe and environmentally-benign since it needs only water, dioxygen, and solar light. Most of metal oxide semiconductors that are widely employed for

photosynthetic and photocatalytic conversions are active under UV light region only, and H_2O_2 having a strong affinity to the oxide surface decomposes as soon as it is produced.[7,8] Recently, a relatively high photo-conversion efficiency of H_2O_2 production was observed over polymeric CN since tri-s-triazine moieties consisting of CN polymeric matrix accelerate a selective two electron transfer to O_2 via the formation of superoxo radical and 1,4-endoperoxide species sequentially.[9] Moreover, the photoefficiency of bare CN for H_2O_2 production could be enhanced through the modification of bandgap (by incorporation of pyromellitic diimide into polymeric CN matrix)[10] and surface properties (by amine rich mesoporous structure) of CN.[11] In this work, potassium, phosphorus, and oxygen elements were simply introduced into polymeric CN matrix by solid-state thermal polymerization of melamine in the presence of potassium phosphate dibasic (KPD, K_2HPO_4). Not only the surface catalytic behaviour induced by the phosphate species but also the formation of charge trapping sites originated from hetero-elements existing over polymeric CN matrix, established a high apparent quantum efficiency (AQE) for H_2O_2 production without adding any noble metal cocatalysts.

2. Results and Discussion

2.1. Hetero-Elements (K, P, and O) Incorporated CN Polymeric Structure

The X-ray diffraction (XRD) patterns in Figure 1a show that the in-situ incorporation of hetero-elements into CN framework induced a significant reduction

of the typical peaks of CN (at 27.5^{o} and 13.0^{o}), ascribed to the interlayer (002) stacking and the interplanar structural packing of tri-s-triazine units forming 1-dimensional melon strands, respectively.[12] According to the KPD content added (x mmol; x = 1, 3, 5, 7.5, and 10), the samples are noted as KPD-CN-1, 3, 5, 7.5, and 10, respectively. When the KPD content increased from x = 1 to 10 at 550 ^{o}C, the peak intensity at 13.0^{o} and 27.5^{o} gradually decreased (Figure S1a), which indicates that the polymeric structure of KPD-CN-x is possibly derived from the simultaneous condensation of melamine and KPD. Basically, prior to reaching the sublimation temperature of melamine (350 ^{o}C), the condensed melamine phosphates consisting of various phosphate species such as orthophosphate, pyrophosphate, polyphosphate, and polymethaphosphate can be generated by the step-by-step condensation reaction,[13] which are known as a halogen-free flame retardant with an excellent thermal resistance.[14] In the case of sole melamine, melamine-based products are dominant up to 350 ^{o}C, but tri-s-triazine (melem) starts to be generated as a result of melamine rearrangement over 350 ^{o}C.[15] With further increase of the temperature, the condensation of tri-s-triazine to polymeric networks induces the formation of CN around 520 ^{o}C, and the decomposition is started to be proceeded above 600 ^{o}C. The XRD pattern of KPD-CN-7.5 exhibits that the melamine and KPD peaks disappeared with increasing the calcination temperature (Figure S1b), and any trace peaks of original melamine and KPD were not observed at all (Figure S1c and S1d). The result supports that the hetero-elements were well incorporated into the CN framework without leaving melamine or KPD compound unreacted.

Diffuse reflectance UV-visible spectra (DRS) demonstrates that the incorporation of KPD into CN increased the absorbance over UV light region, whilst the change of visible light absorption was almost negligible (Figure 1b and Figure S2a). As a result, the difference of bandgap size between CN and KPD-CN-7.5 was estimated to be only about 0.08 eV. To confirm the shift of the CB and VB potential affected by KPD, the X-ray photoelectron spectroscopy (XPS) VB analysis and the electrochemical Mott-Schottky analysis were carried out. The VB maximum edges of CN and KPD-CN-7.5 are determined to be about 1.75 and 1.86 eV, respectively (Figure 1c), and the Mott-Schottky plots showing n-type characteristics (positive slope) of CN and KPD-CN-7.5 are almost the same (Figure 1d). Contrary to the previous studies on bandgap-engineered CN which clearly showed the bandgap size decrease/increase and the shift of the CB/VB potential as well,[16] the hetero-elements did not markedly change their electronic band structure.

As presented in Figure 2a and Table S1, the typical C-N peaks of CN between 1200 and 1600 cm^{-1} were little changed in KPD-CN-7.5. The incorporation of potassium ions into CN framework shifted the stretching modes of tri-s-triazine ring at 1393 and 1538 cm^{-1} to 1404 and 1571 cm^{-1}, respectively, due to a strong ion-dipole interaction at the nitride pots.[4,17] Similar with chelation, metal ions including cobalt, manganese, potassium, iron, etc. can be coordinated with nonbonding electrons of nitrogen in the nitride pots (pore induced by trigonal bonding of tri-s-triazines).[4, 17] The P-relevant peak of phosphate at 847 and 984 cm^{-1} and the P-O-C stretching at 903 and 1146 cm^{-1} were newly formed and these peaks became

predominant with increasing KPD content (Figure S2b).[18-20] On the other hand, the out-of-plane bending mode (also assigned as the deformation mode of N-H) at 888 cm^{-1} completely disappeared.[21,22] The result indicates that potassium ions and phosphate species are well-assembled inside polymeric CN matrix.

The surface property of CN and KPD-CN-7.5 was also evaluated by zeta-potential analysis since the primary ($C-NH_2$), secondary (C-NH-C), and tertiary (C_3N) amines present in CN can be protonated and deprotonated depending on pH.[23] The CN exhibits the point of zero charge (PZC) at around pH 3 (Figure 2b). However, KPD-CN-7.5 predominantly carries negative charge over the entire pH range from 1 to 11 without showing PZC in terms of phosphate species.

To analyze the chemical states for each carbon, nitrogen, potassium, phosphorus, and oxygen element consisting of CN and KPD-CN-7.5, a high-resolution XPS analysis was carried out. As shown in Figure 2c and Figure S3b, the K2p peaks were clearly observed at 292.6 and 295.4 eV in KPD-CN-7.5 since potassium ions were coordinated with nonbonding electrons of nitrogen via ion-dipole interaction, which is analogous to the molecular structure of metalloporphyrin and $KMnO_4$•18-crown-6-ether.[24,25] In Figure S3a and S3b, the C1s peaks were deconvoluted into six components in both CN and KPD-CN-7.5. Each deconvoluted peak (C1-6, N1-5, and O1-3) is denoted in Table S2. The relative intensity of the C2, C5, and C6 peaks increased along with the decrease of C4 intensity, which revealed that more carbon sites were interacted or replaced by the oxygen atoms present in phosphate species. Furthermore, the binding energy of C4 was positively shifted (0.2 eV) due to higher

electronegativity of oxygen than nitrogen, and the formation of cyano group increased the C3 peak intensity. In the case of N1s spectra (Figure S3c and S3d), the ratio of N2 to (N3 + N4) was calculated as 2.12 in CN and 2.43 in KPD-CN-7.5, respectively. The N2 mainly participates in the build-up of bandgap structure but the N3 and N4 are in charge of bulk and surface properties so it can be concluded that the surface properties induced by protonated N3 and N4 are less accessible.[26] The elemental XPS C/N ratio (Table S3) and elemental C/N ratio obtained by elemental analysis (Table S4) of CN steadily decreased with increasing the atomic percent of phosphorus and oxygen. Although the C/N ratio of bulk CN is not consistent between the elemental XPS and elemental C/N analysis (the real C/N ratio can be changed by the experiment conditions[27,28]), the decrease trend is the same in both cases. The P2p band was absent in CN and the single symmetric peak at 132.9 eV was observed in KPD-CN-7.5 (Figure S3e and S3f), which indicates that P in KPD-CN-7.5 is mainly combined with O instead of C and N (since P2p binding energy of P-C, P-O, and P-N is about 131.0, 132.9, and 133.5 eV, respectively[29-31]). As a result, the phosphate incorporation in the CN matrix induced the appearance of the O1s peak centered at 531.0 eV that is absent in CN (Figure S3g and S3h).

Solid-state ^{31}P magic angle spinning (MAS) nuclear magnetic resonance (NMR) spectra of CN and KPD-CN-7.5 are compared in Figure 2d. While no peak is observed at all in CN, a broad peak from 17 to -50 ppm (δ_{max} = -11.6 ppm) and spinning side bands are clearly shown in KPD-CN-7.5. In general, the chemical shifts on phosphate monoester, orthophosphate, phosphate diester, pyrophosphate,

and polyphosphate are normally observed around at $0 \leq \delta \leq 10$, $0 \leq \delta \leq 5$, $0 \leq \delta \leq -5$, $-5 \leq \delta \leq -10$, and $-10 \leq \delta \leq -30$ ppm, respectively.[32,33] Furthermore, there is no prominent chemical shift induced by the phosphonate group (C-P) usually observed over 20 ppm. The result supports that the phosphate species do not exist as a sole compound, but various species are incorporated into the complex CN matrix. Solid-state proton-decoupled ^{13}C cross polarization and magic angle spinning nuclear magnetic resonance (CP-MAS NMR) spectrum of CN exhibited two evident signals (Figure S4). The strong peak recorded at 164.7 ppm belongs to the terminal carbon (N_2-C-NH_2 groups), and the second peak at 157.0 ppm is ascribed to the internal carbon (C-$(N)_3$ groups).[34] The ^{13}C CP-MAS NMR spectrum of KPD-CN-7.5 also revealed two signals centered at 163.9 and 156.6 ppm. The quantitative intensity analysis of CP-MAS NMR signals is not reliable but the number of signals and their relative ratio provide the useful information. The ratio of the terminal carbon to the internal one of CN and KPD-CN-7.5 was measured as 1.55 and 2.88, respectively. Considering the decrease of C/N ratio in KPD-CN-7.5, the replacement of carbon atoms could occur on the internal carbon sites and the formation of C-O-P bond might take place on the terminal sites.

The morphologies and the chemical composition of CN and KPD-CN-7.5 were confirmed by high resolution transmission electron microscope (HR-TEM) and energy-dispersive X-ray spectroscopy (EDS) analysis, respectively. The EDS mapping confirmed the presence of predominant carbon and nitrogen, and the small amount of oxygen as well, but any potassium and phosphorus was not measured at

all in CN (Figure 3b-3f). However, in the case of KPD-CN-7.5, carbon, nitrogen, potassium, phosphorus, and oxygen were homogeneously dispersed over the materials (Figure 3h-3l). To further characterize the properties of CN and KPD-CN-7.5, the BET surface area and pore volume measurement (Figure S5a), thermogravimetric analysis (Figure S5b), and field-emission scanning electron microscopy (Figure S6) were carried out (see Supporting Information regarding the detailed result discussion).

2.2. Photocatalytic Production of H_2O_2

First of all, it should be mentioned that the present study is not an ideal photosynthesis of H_2O_2 that utilizes water and O_2 only since an excess of ethanol was used as an electron donor instead of water. Considering the standard reduction potentials of O_2 reduction ($E^0(O_2/H_2O_2)$ = 0.695 V_{NHE}) and ethanol oxidation ($E^0(CO_2/C_2H_5OH)$ = 0.085 V_{NHE}), the overall process of H_2O_2 production in the present study is thermochemically spontaneous (that is, *photocatalytic*, not *photosynthetic*). The main focus of this work is to investigate the effects of hetero-elements on the half reaction of H_2O_2 production via O_2 reduction, not to establish the ideal photosynthesis. On the other hand, the ethanol oxidation coupled with the production of H_2O_2 was not analysed in this work because the photoreaction was carried out under continuous O_2 purging condition, which should volatilize the products of ethanol oxidation immediately from the solvent. However, in a previous study which utilized pure CN for the photochemical production of H_2O_2 in

ethanol/water solvent in a closed reactor,[9] most of ethanol was oxidized to acetaldehyde with almost stoichiometric production of H_2O_2 with a molar ratio of 1:1 (*i.e.,* $O_2 + CH_3CH_2OH \rightarrow H_2O_2 + CH_3CHO$). The ethanol oxidation part should be similar in this study as well.

The photoactivity was tested by monitoring the visible light-induced production of H_2O_2. The photo-production of H_2O_2 was compared among the CN and KPD-CN-x (x=1, 3, 5, 7.5, and 10) samples in the presence of ethanol as an electron donor in the O_2-saturated catalyst suspension under visible light irradiation ($\lambda \geq 420$ nm) (Figure S7a). All KPD-CN-x samples exhibited markedly enhanced activities compared with CN although the specific surface areas of all KPD-CN-x samples are significantly lower than bare CN (*see* Figure S5a). This indicates that the surface area of the catalyst samples is not an important factor and that the enhancement of the photocatalytic activity should be ascribed to other modified properties (*e.g.,* charge recombination, separation and interfacial transfer, nature of catalytic active sites) induced by the incorporation of potassium and phosphate species. The photoactivity for H_2O_2 production increased with increasing KPD content and reached a maximum at x=7.5. Therefore, the KPD-CN-7.5 was chosen as an optimal sample for further experiments. To investigate the wavelength dependence of the H_2O_2 production, the AQY was measured using a monochromatic light (λ = 320, 370, 420, 470, and 520 nm) irradiation. As shown in Figure 4a, AQY for the production of H_2O_2 at 320 nm and 420 nm in KPD-CN-7.5 was 17 and 25 times higher than that of CN, respectively. In addition, the turnover frequency (TOF) of the KPD-CN-7.5

at 320 nm and 420 nm was 49.8 and 73.1 times higher than that of CN, respectively. Considering that the production of H_2O_2 requires a PCET process, KPD-CN-7.5 is advantageous since it has phosphate functionalized polymeric structure, which can facilitate a proton transfer process.[16,35-37] Since the production of H_2O_2 via PCET should be highly dependent on the proton concentration, it decreased with increasing pH (Figure S7b). The production of H_2O_2 at pH 1.0 was more than doubled from that at pH 3.0 for CN while the enhancement factor ($[H_2O_2]_{pH=1}/[H_2O_2]_{pH=3}$) was only 1.1 for KPD-CN-7.5. The proton transfer in KPD-CN-7.5 was facilitated enough by the presence of the phosphate species, and therefore, a higher concentration of proton (at lower pH) has a relatively lower enhancement effect on the production of H_2O_2 than in the case of CN. Moreover, KPD-CN-7.5 exhibited much higher photoactivities than CN up to pH 9.0. To check the product selectivity for H_2O_2 compared to H_2, the H_2 evolution test was also carried out in the presence of ethanol in a tightly-sealed reactor under Ar(g) atmosphere under UV light irradiation for 12 h. Both CN and KPD-CN-7.5 evolved a very tiny amount of H_2 (below 0.1 μmol), which supports that two-electron transfer to O_2 coupled with protons (Table S5, eq. 5: $O_2 + 2H^+ + 2e^- \rightarrow H_2O_2$) is much more favored than the direct two-electron transfer to protons (Table S5, eq. 18: $2H^+ + 2e^- \rightarrow H_2$).

The photoactivity tests with CN and KPD-CN-7.5 were performed in air-, Ar-, and O_2-saturated suspensions to verify the role of dioxygen for the photoproduction of H_2O_2 (Figure 4b). In general, the photo-excited CB electrons can be scavenged by dissolved O_2 in air- or O_2-saturated condition but the protons should uptake the

electrons in the absence of O_2 (Ar-atmosphere). The rate of H_2O_2 formation on KPD-CN-7.5 was markedly enhanced in the O_2-saturated suspension from that in the air-saturated one. While the $[H_2O_2]_{O2}/[H_2O_2]_{air}$ at 3 h was measured to be 1.7 for KPD-CN-7.5, it was 1.2 for CN. Under Ar-saturated condition, no H_2O_2 was formed not only with CN but also with KPD-CN-7.5, which confirms that H_2O_2 is generated through the reduction of O_2. The KPD-CN-7.5 was stable enough to maintain the photocatalytic activity during the repeated cycles of H_2O_2 production as shown in Figure 4c. On the other hand, it should be noted that the overall production of H_2O_2 is determined by the photocatalytic decomposition of H_2O_2 as well as its production since the photogenerated H_2O_2 can be subsequently decomposed on the photocatalyst surface. Therefore, the overall photoconversion efficiency can be enhanced not only by facilitating the photoreduction of O_2 but also by inhibiting the decomposition of H_2O_2 on the photocatalyst surface. For example, our recent study demonstrated that the modification of TiO_2 surface by phosphate loading inhibited the adsorption of H_2O_2 with significantly retarding the photodecomposition of H_2O_2, which resulted in a highly enhanced production of H_2O_2.[6] In this respect, KPD-CN-7.5 is much better than TiO_2 for H_2O_2 production because the adsorption of H_2O_2 on the former is negligible but the latter shows some adsorption affinity for H_2O_2 [Adsorption of 100 μM H_2O_2 in the dark under continuous stirring for 0.5 h: $[H_2O_2]_{ad}$ = 0 μM for KPD-CN-7.5 (surface area: 3.4 m^2/g) *vs.* $[H_2O_2]_{ad}$ = 12.1 μM for TiO_2 (surface area: 47 m^2/g); *Although the surface area of the tested TiO_2 is higher than KPD-CN-7.5, the higher adsorption of H_2O_2 on TiO_2 should be ascribed*

mainly to the strong surface complexation of H_2O_2 on TiO_2 (>Ti(IV)-OH)$_{surf}$ + H_2O_2 → (>Ti(IV)–OOH)$_{surf}$ + H_2O)] As a result, CN and KPD-CN-7.5 did not degrade H_2O_2 at all under visible light ($\lambda \geq 420$ nm) (Figure S7c). Under UV irradiation ($\lambda \geq 320$ nm), on the other hand, CN exhibited some activity for H_2O_2 decomposition but KPD-CN-7.5 did not degrade H_2O_2 at all. The inactivity of KPD-CN-7.5 for the decomposition of H_2O_2 should also contribute to the higher activity of KPD-CN-7.5 than CN. In addition, the production of H_2O_2 was highly affected by not only the type of the electron donor (2-propanol > ethanol > methanol >> water) (Figure S8a and S8b) but also the ratio of alcohol to water (Figure S8c). With CN, the photocatalytic production of H_2O_2 was dramatically inhibited by increasing the water content (from 10% to 90%) whereas that of KPD-CN-7.5 was less affected by increasing the water content. That is, KPD-CN-7.5 should be much more favoured than CN for the production of H_2O_2 in water-rich environment.

2.3. Charge Transfer Dynamics

The charge separation behaviour of carbon nitrides was investigated by steady-state photoluminescence (PL), time-resolved PL (TRPL), slurry-type photocurrent measurement, and time-resolved diffuse reflectance spectroscopy using femtosecond laser. As shown in Figure 5a, the radiative recombination of excited charge pairs was clearly observed in CN while the PL intensity was markedly reduced with increasing KPD content, which indicates that the radiative recombination is much retarded in KPD-CN-7.5 compared with CN. The wavelength dependent PL emission intensity

for CN, KPD-CN-3, KPD-CN-7.5 reveals that the PL intensity linearly enhanced with increasing the excitation wavelength for all samples since the excitation light intensity has a linear correlation with the excitation wavelength as well (Figure S9). However, the slope linearly decreased with increasing KPD content, which implies that the hetero-elements effectively prohibit the radiative recombination through the formation of charge trapping sites. The PL excitation spectrum detected at 470 nm for CN shows three distinct PL bands at 271, 367, and 429 nm together with a broad background signal (Figure 5b). Although the PL band at 271 nm was not observed and the background signal was weak in KPD-CN-7.5, the other two PL bands were still visible. The result supports that the hetero-elements generate the trapping sites for charge carriers rather than the change of band structure. The mobile electrons and holes produced by the excitons can freely diffuse or can be shallowly trapped over the polymeric CN lattice in CN, whereas the charge carriers can be deeply trapped and then the non-radiative recombination markedly takes place in KPD-CN-7.5. Furthermore, it is quite probable that the recombination can be facilitated by the decrease of CN wt% with increasing KPD content (Table S4) since the radiative recombination occurs in polymeric CN matrix. Therefore, the average lifetime of charge carriers in CN, KPD-CN-3, and KPD-CN-7.5 was estimated by fitting the decay curve with three exponential terms to yield 2.51, 1.68, 0.83 ns, respectively (Figure 5c). The interfacial electron transfer was also investigated by measuring the $PW_{12}O_{30}^{3-/4-}$ redox couple (E^o = +0.22 V_{NHE})-mediated photocurrent collected in the visible light-irradiated suspension of catalysts.[38] Figure 5d shows that the time

profiles of photocurrent generation were enhanced with KPD-CN-7.5 in comparison with CN, which is consistent with the higher visible light activity of KPD-CN-7.5.

To directly observe the presence of charge trapping sites on CN, KPD-CN-3, and KPD-CN-7.5, time-resolved diffuse reflectance spectra were measured. To avoid the precipitation problem occurring in aqueous suspension, all samples were homogeneously coated on glass slide and reflectance change induced by laser excitation was measured. Until now, few transient absorption spectroscopic studies were done for CN (protonated CN,[28] colloidal CN,[27] mesoporous CN,[39] and polymeric CN[40]), so more depth investigation is highly required. In this study, we focused on the lifetime of transient species formed by trapped charge carriers to confirm the role of hetero-elements incorporated in CN framework. As shown in Figure 6, the broad positive absorption band was similarly observed for all samples after laser pulse at 400 nm under air. Recently, Zhang et al. reported that the positive absorption was attributed to the formation of charge separation states by photogenerated electron/hole pairs in colloidal CN system.[27] Kuriki et al. also defined that the broad positive absorption was originated from deeply trapped electron/hole pairs.[39] The transient absorption decay for charge separation states was well fitted by the biexponential equation for all samples, and the average lifetime of CN, KPD-CN-3, and KPD-CN-7.5 was calculated as 353.1, 477.7, and 1194.0 ps, respectively. Although the transient absorption intensity was a little reduced in KPD-CN-7.5 relative to CN due to less wt% of CN content, the charge separation process is improved by the hetero-elements. The results support that the incorporation of

hetero-elements into polymeric CN matrix could generate not only the extra charge trapping sites but also the catalytic sites favourable to the PCET process, which should influence the recombination kinetics and the interfacial charge transfer characteristics to facilitate the photoproduction of H_2O_2.

2.4. Other Hetero-Elements Incorporated CN Materials

Other chemicals instead of KPD were employed as alternative reagents to investigate the cationic and anionic effects on the photocatalytic production of H_2O_2 systematically and their XPS elemental analysis was also carried out (Figure 7 and Table S6). When the ratio of proton to potassium was changed using H_3PO_4, KH_2PO_4, K_2HPO_4, and K_3PO_4, the relative percentage of potassium, phosphorus, and oxygen consisting of the samples increased in the order K_3PO_4 > K_2HPO_4 > KH_2PO_4 > H_3PO_4. However, the highest photocatalytic activity was obtained with K_2HPO_4 instead of K_3PO_4 because the polymeric CN matrix was decomposed in the presence of K_3PO_4 (the C/N ratio = 0.32) (Figure 7a). No potassium was found in the sample when H_3PO_4 was used. On the other hand, when H_2SO_4, $KHSO_4$, and K_2SO_4 were employed as alternative reagents, the potassium content in the CN matrix was in the order of K_2SO_4 > $KHSO_4$ > H_2SO_4 but no sulfur element was found in the samples. The highest photocatalytic activity was obtained with $KHSO_4$, but the amount of H_2O_2 produced was lower than that of KPD-CN-7.5 (Figure 7b). The result demonstrated that KPD is a good source to incorporate both phosphate species and potassium ions into the CN matrix. As for the cation effect, different dihydrogen

phosphate reagents containing various cations were also tested and compared for the photocatalytic activities for H_2O_2 production, which exhibited the reactivity order of KH_2PO_4 > NaH_2PO_4 > LiH_2PO_4 > H_3PO_4 > $(NH_4)H_2PO_4$ (Figure 7c). When different anions (HCO^{3-}, HSO^{4-}, and $H_2PO_4^{2-}$) combined with potassium ion were tested, the best photocatalytic activity was obtained with $H_2PO_4^{2-}$ (Figure 7d). Among various combinations of cationic and anionic species for the incorporation into the CN matrix, the combination of potassium and dihydrogen phosphate in KPD-CN-7.5 showed the best photocatalytic performance.

3. Conclusions

Despite the simple synthetic procedure for CN, its polymeric structure is still controversial (even s-heptazine has been recently considered as a basic building block) and the synthetic mechanism is not fully understood.[41] Therefore, it does not make much sense to conclude the exact structure and synthetic mechanism in the present case of modified CN. However, the analyses using various spectroscopic methods revealed that the earth-abundant hetero-elements (K, P, and O) could be incorporated into the carbon nitride framework via thermal polymerization to modify the surface and charge transfer properties significantly and consequently to enhance the photoactivities for the production of H_2O_2. According to DRS, XPS, and Mott-Schottky plots, the incorporation of the multiple hetero-elements does not affect the bandgap size and the band potential shift. The presence and chemical states of the

hetero-elements were confirmed by FT-IR, Zeta-potential analysis, XPS, solid state NMR, and EDX mapping, which comes to conclusions that 1) potassium is captured as an ion by non-pair electrons of nitrogen present in CN matrix, 2) phosphorus and oxygen elements exist as various phosphate species, and 3) carbon sites are attacked by the oxygen present in the phosphate species relative to nitrogen sites. The high photoactivity of KPD-CN-7.5 and particularly high selectivity toward H_2O_2 over H_2 are attributed to 1) the enhanced light absorption (UV light region), 2) the increased lifetime of the transient species, 3) the effective interfacial charge transfer to dioxygen via PCET, and 4) the inhibited decomposition of in-situ generated H_2O_2. It should be noted that such unique activity and selectivity for H_2O_2 production cannot be an additive property of K-doped CN and P-doped CN at all (*see* Figure 7). The KPD-modified CN is uniquely suited for the photochemical production of H_2O_2. The incorporation of various earth-abundant elements into CN could be also possible for a variety of applications. This study clearly demonstrated that the hetero-elements incorporated CN can be exploited for cost-effective and environment-friendly photocatalysts without utilizing any noble metals, which should be important for the development of practical and economical solar conversion photocatalytic materials.

4. Experimental Section

Materials preparation: To synthesize CN, 4 g of melamine (99%, Aldrich) in a porcelain cup covered with a cap was calcined at 550 ^{o}C for 4 h (heating and cooling rate was 2.2 ^{o}C/min, respectively.). After grinding the CN sample homogeneously, the aqueous solution containing CN (1 g/L) was sonicated in an ultrasonic bath (JAC 4020, 400 W, Sonic) for 3 h, filtered, washed, and finally dried at room temperature. Modified CN compounds were prepared through a similar synthetic procedure of CN. 4 g of melamine and each 1, 3, 5, 7.5, and 10 mmol of KPD (K_2HPO_4 99.95%, Aldrich) were homogeneously ground, respectively. On the basis of 7.5 mmol, 4 g of melamine was mixed and ground with phosphoric acid (85 wt.% in water, Aldrich), potassium phosphate monobasic (99.99%, Aldrich), potassium phosphate tribasic (98%, Aldrich), sulfuric acid (95.0-98.0%, Aldrich), potassium bisulfate (99%, Aldrich), potassium sulfate (99.99%, Aldrich), ammonium phosphate monobasic (99.999%, Aldrich), lithium phosphate monobasic (99.99%, Aldrich), sodium phosphate monobasic (99.0%, Aldrich), and potassium bicarbonate (99.95%, Aldrich), respectively. Phosphoric acid or sulfuric acid mixed melamine powder was dried at 80 ^{o}C for 3 h to remove water and then was ground again. The other procedure is the same with CN synthetic procedure.

Photocatalytic activity tests: 20 mg of each sample was dispersed in the solution containing 36 mL of purified water and 4 mL of ethanol by ultra-sonication. The pH of the suspension was controlled by $HClO_4$ or KOH. Before the irradiation, the suspension was stirred under O_2 purging for 30 min to make it O_2-saturated. The reactor was irradiated by a

300-W Xe arc lamp (Oriel) under continuous stirring and purging. Light was passed through a 10-cm IR filter and a cutoff filter ($\lambda \geq 420$ nm or $\lambda \geq 320$ nm), and then was focused onto the reactor. The intensity of the incident light filtered through cutoff filters ($\lambda \geq 420$ nm and $\lambda \geq 320$ nm) was determined to be about 726.8 mW/cm^2 and 833 mW/cm^2, respectively, which was measured by a power meter (Newport 1830-C).

To calculate the apparent quantum yield (AQY), the incident light was passed through a SAP301 grating monochromator (Newport, Oriel 77250). The light intensity was measured using an optical power meter (1815-C, Newport) with a photodiode detector (818-UV, Newport). The light intensity at 320, 370, 420, 470, and 520 nm was measured as 0.16, 0.40, 0.74, 1.06, and 0.75 mW, respectively. AQY was estimated from the formula of $\Phi_{AQY}(\%)$ = (Number of H_2O_2 formed x 2)/ (Number of incident photons) x 100. The turnover number was calculated after 6 h irradiation. The number of C_6N_8 units on the surface was assumed as 7.55 x 10^{-5} mol/g in both CN and KPD-CN-7.5. The C_6N_8 unit per area was 0.22 nm^{-2}, and the surface area of CN and KPD-CN-7.5 was 10 and 3.4 m^2/g, respectively.

The recycle test was performed as follows. 20 mg of the sample was dispersed in the solution containing 36 mL of purified water and 4 mL of ethanol (pH_i = 3), which was irradiated at $\lambda \geq 420$ nm under continuous O_2 purging condition. After 1st cycle, the suspension was filtered, washed, and then re-dispersed in the solution (0.5 g/L of the photocatalyst and 10 vol.% of ethanol) by ultra-sonication. The same procedure was repeated up to 4th cycle. The photocatalytic decomposition of H_2O_2 with using bare CN and KPD-CN-7.5 was carried out as follows: 0.5 g/L of the photocatalyst was dispersed in the

solution containing 5 mM of H_2O_2 at pH 3.0. Before the irradiation, the suspension was kept in dark for 30 min and then visible ($\lambda \geq 420$ nm) or UV light ($\lambda \geq 320$ nm) was sequentially irradiated under continuous O_2 purging condition. Methanol and 2-propanol were also tested as an alternative electron donor. The photocatalytic H_2 evolution was tested as well to estimate the selectivity toward H_2O_2 by a gas chromatograph (GC, HP6890N) with a thermal conductivity detector.

Supporting Information

Experimental details, characterizations of KPD-CN-x (x = 0, 1, 3, 5, 7.5, and 10) (XRD, DRUVS, FT-IR, high resolution XPS, ^{13}C CP-MAS NMR, BET surface area & pore volume, TGA, FE-SEM, steady-state photoluminescence, and elemental analysis), the photocatalytic generation of H_2O_2 depending on KPD content, pH, and electron donors, and the photocatalytic decomposition of H_2O_2 under UV and visible irradiation. This material is available free of charge via the Internet at http://pubs.acs.org.

Acknowledgements

This work was financially supported by the Global Research Laboratory (GRL) Program (No. NRF-2014K1A1A2041044) and KCAP (Sogang Univ.) (No. 2009-0093880), which were funded by the Korea Government (MSIP) through the National Research Foundation (NRF).

References

(1) Colmenares, J. C.; Luque R. *Chem. Soc. Rev.* **2014**, *43*, 765-778.
(2) Park, H.; Kim, H. I.; Moon, G. H.; Choi, W. *Energy Environ. Sci.* **2016**, *9*, 411-433.
(3) Wang, Y.; Wang, X. C.; Antonietti, M. *Angew. Chem.-Int. Edit.* **2012**, *51*, 68-89.
(4) Cao, S.; Low, J.; Yu, J.; Jaroniec, M. *Adv. Mater.* **2015**, *27*, 2150-2176.
(5) Campos-Martin, J. M.; Blanco-Brieva, G.; Fierro, J. L. G. *Angew. Chem.-Int. Edit.* **2006**, *45*, 6962-6984.
(6) Moon, G. H.; Kim, W.; Bokare, A. D.; Sung, N. E.; Choi, W. *Energy Environ. Sci.* **2014**, *7*, 4023-4028.
(7) Hoffmann, M. R.; Martin, S. T.; Choi, W.; Bahnemann, D. W. *Chem. Rev.* **1995**, *95*, 69-96.
(8) Maurino, V.; Minero, C.; Mariella, G.; Pelizzetti, E. *Chem. Commun.*, **2005**, 2627-2629.
(9) Shiraishi, Y.; Kanazawa, S.; Sugano, Y.; Tsukamoto, D.; Sakamoto, H.; Ichikawa, S.; Hirai, T. *ACS Catal.* **2014**, *4*, 774-780.
(10) Shiraishi, Y.; Kanazawa, S.; Kofuji, Y.; Sakamoto, H.; Ichikawa, S.; Tanaka, S.; Hirai, T. *Angew. Chem.-Int. Edit.* **2014**, *53*, 13454-13459.
(11) Shiraishi, Y.; Kofuji, Y.; Sakamoto, H.; Tanaka, S.; Ichikawa, S.; Hirai, T. *ACS Catal.* **2015**, *5*, 3058-3066.
(12) Wang, X. C.; Maeda, K.; Thomas, A.; Takanabe, K.; Xin, G.; Carlsson, J. M.; Domen, K.; Antonietti, M. *Nat. Mater.* **2009**, *8*, 76-80.
(13) Cichy, B.; Luczkowska, D.; Nowak, M.; Wladyka-Przybylak, M. *Ind. Eng. Chem. Res.* **2003**, *42*, 2897-2905.
(14) Cichy, B.; Kuzdzal, E. *Ind. Eng. Chem. Res.* **2012**, *51*, 16531-16536.
(15) Thomas, A.; Fischer, A.; Goettmann, F.; Antonietti, M.; Müller, J.-O.; Schlögl, R.; Carlsson, J. M. *J. Mater. Chem.* **2008**, *18*, 4893-4908.
(16) Chu, S.; Wang, Y.; Guo, Y.; Feng, J.; Wang, C.; Luo, W.; Fan, X.; Zou, Z. *ACS Catal.* **2013**, *3*, 912-919.
(17) Gao, H.; Yan, S.; Wang, J.; Huang, Y. A.; Wang, P.; Li, Z.; Zou, Z. *Phys. Chem. Chem. Phys.* **2013**, *15*, 18077-18084.
(18) Khabashesku, V. N.; Zimmerman, J. L.; Margrave, J. L. *Chem. Mater.* **2000**, *12*, 3264-3270.
(19) Miller, F. A.; Wilkins, C. H. *Anal. Chem.* **1952**, *24*, 1253-1294.
(20) Yang, Z.; Wang, Z.; Li, J.; Chen, J. *RSC Adv.* **2012**, *2*, 11432-11437.
(21) Huang, Y.; Wang, Y.; Bi, Y.; Jin, J.; Ehsan, M. F.; Fu, M.; He, T. *RSC Adv.* **2015**, *5*, 33254-33261.
(22) Dong, F.; Wang, Z.; Sun, Y.; Ho, W. K.; Zhang, H. *J. Colloid Interface Sci.* **2013**, *401*, 70-79.
(23) Zhu, B. C.; Xia, P. F.; Ho, W. K.; Yu, J. G. *Appl. Surf. Sci.* **2015**, *344*, 188-195.
(24) Hu, S.; Li, F.; Fan, Z.; Wang, F.; Zhao, Y.; Lv, Z. *Dalton Trans.* **2015**, *44*, 1084-1092.
(25) Moulder, J. F.; Stickle, W. F.; Sobol, P. E.; Bomben, K. *Handbook of X-ray Photoelectron Spectroscopy*, 2nd ed.; Perkin-Elmer, Physical Electronics Division: Eden Prairie, MN, **1992**.
(26) Martin, D. J.; Qiu, K.; Shevlin, S. A.; Handoko, A. D.; Chen, X.; Guo, Z.; Tang, J. *Angew. Chem.-Int. Edit.* **2014**, *53*, 9240-9245.
(27) Zhang, H. Y.; Chen, Y. P.; Lu, R.; Li, R. Y.; Yu, A. C. *Phys. Chem. Chem. Phys.* **2016**, *18*, 14904-14910.
(28) Ye, C.; Li, J.-X.; Li, Z.-J.; Li, X.-B.; Fan, X.-B.; Zhang, L.-P.; Chen, B.; Tung, C.-H.; Wu, L.-Z. *ACS Catal.* **2015**, *5*, 6973-6979.
(29) Puziy, A. M.; Poddubnaya, O. I.; Socha, R. P.; Gurgul, J.; Wisniewski, M. *Carbon* **2008**, *46*, 2113-2123.
(30) Gorham, J.; Torres, J.; Wolfe, G.; d'Agostino, A.; Fairbrother, D. H. *J. Phys. Chem. B* **2005**, *109*, 20379-20386.
(31) Zhang, Y. J.; Mori, T.; Ye, J. H.; Antonietti, M. *J. Am. Chem. Soc.* **2010**, *132*, 6294-6295.
(32) Sannigrahi, P.; Ingall, E. D.; Benner, R. *Geochim. Cosmochim. Acta* **2006**, *70*, 5868-5882.
(33) He, Z.; Honeycutt, C. W.; Xing, B.; McDowell, R. W.; Pellechia, P. J.; Zhang, T. *Soil Sci.* **2007**, *172*, 501-515.

(34) Jürgens, B.; Irran, E.; Senker, J.; Kroll, P.; Müller, H.; Schnick, W. *J. Am. Chem. Soc.* **2003**, *125*, 10288-10300.
(35) Kreuer, K. D.; Paddison, S. J.; Spohr, E.; Schuster, M. *Chem. Rev.* **2004**, ***104***, 4637-4678.
(36) Vilciauskas, L.; Tuckerman, M. E.; Bester, G.; Paddison, S. J.; Kreuer, K. D. *Nat. Chem.* **2012**, *4*, 461-466.
(37) Park, H.; Choi, W. *J. Phys. Cehm. B* **2003**, *107*, 3885-3890.
(38) Liu, G.; Wang, T.; Zhang, H.; Meng, X.; Hao, D.; Chang, K.; Li, P.; Kako, T.; Ye, J. *Angew. Chem.-Int. Edit.* **2015**, *54*, 13561-13565.
(39) Kuriki, R.; Matsunaga, H.; Nakashima, T.; Wada, K.; Yamakata, A.; Ishitani, O.; Maeda, K. *J. Am. Chem. Soc.* **2016**, *138*, 5159-5170.
(40) Merschjann, C.; Tschierlei, S.; Tyborski, T.; Kailasam, K.; Orthmann, S.; Hollmann, D.; Schedel-Niedrig, T.; Thomas, A.; Lochbrunner, S. *Adv. Mater.* **2015**, *27*, 7993-7999.
(41) Schwarzer, A.; Saplinova, T.; Kroke, E. *Coord. Chem. Rev.* **2013**, *257*, 2032-2062.

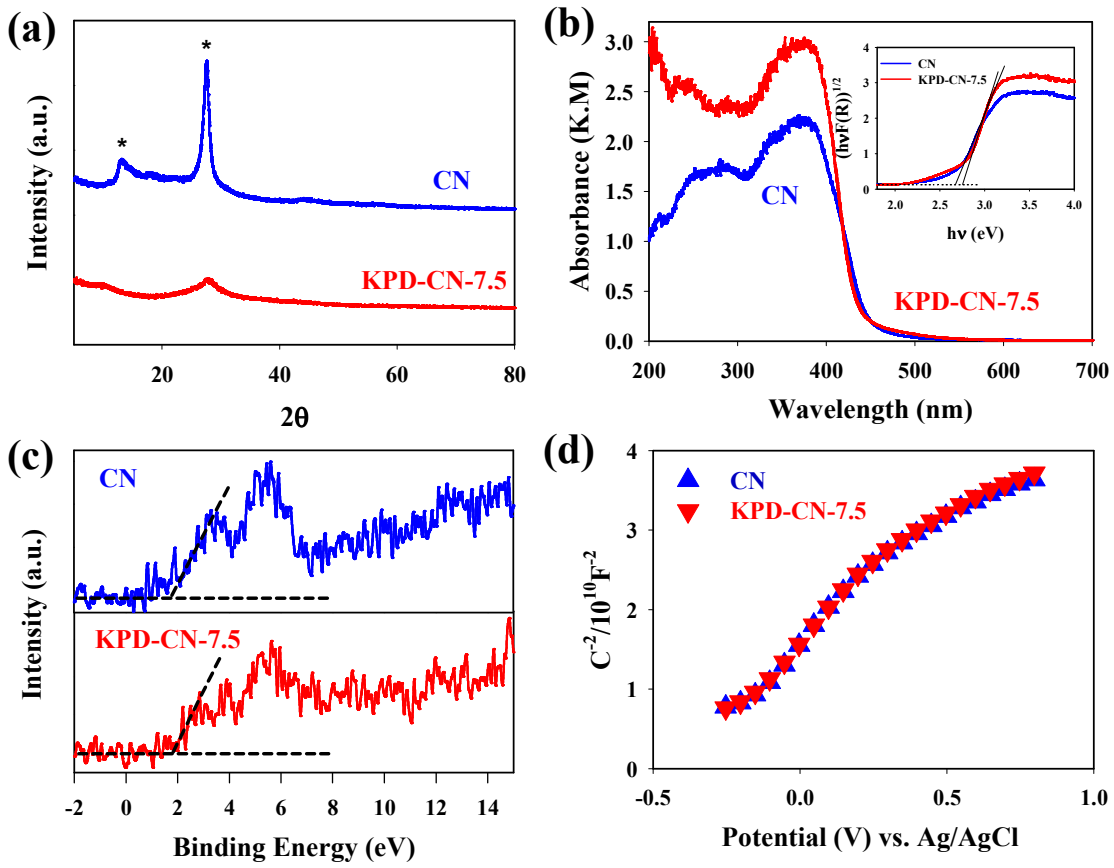

Figure 1. (a) XRD spectra, (b) DRUVS spectra, (c) XPS valence band analysis, (d) Mott-Schottky plots for bare CN and KPD-CN-7.5. Inset in (b): Tauc plot for bare CN and KPD-CN-7.5.

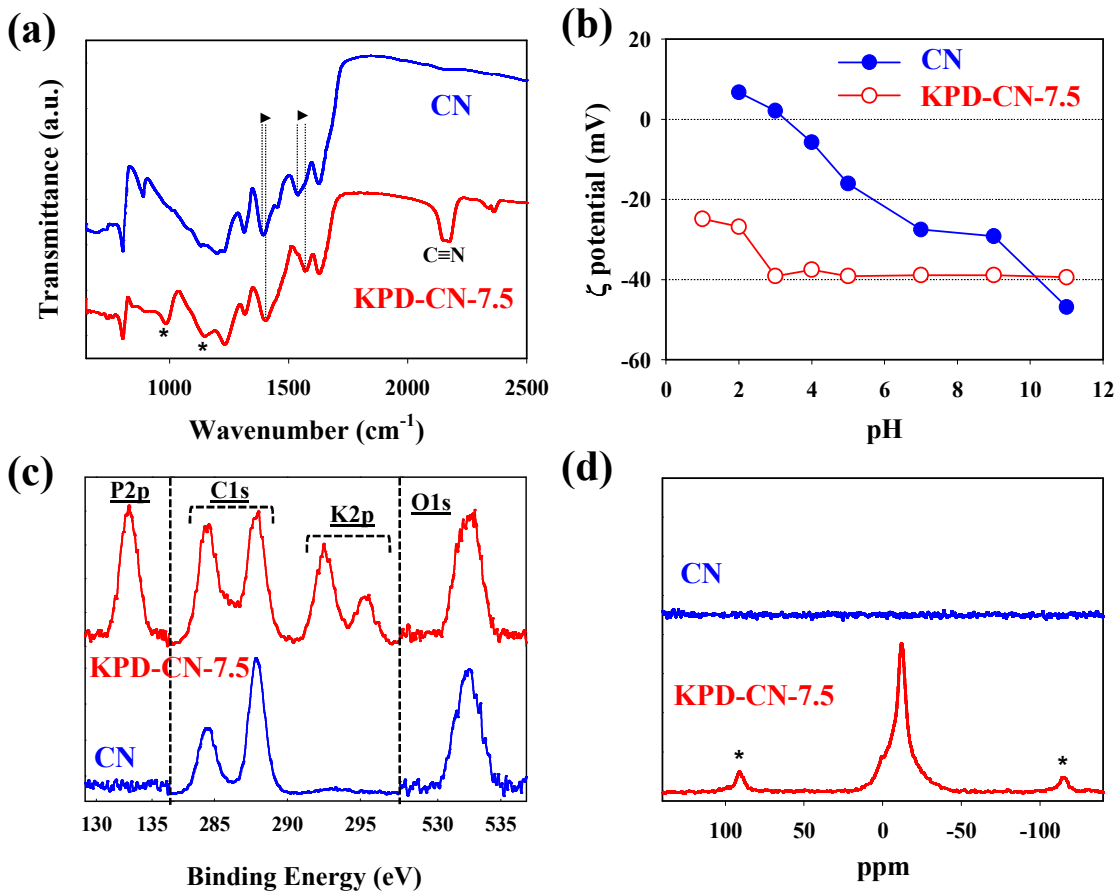

Figure 2. (a) ATR FT-IR spectra (Asterisks indicate the bonding, P-O-C, and the arrows represent the peak shift of typical peaks of CN) of bare CN and KPD-CN-7.5. (b) zeta-potential analysis of bare CN and KPD-CN-7.5. (c) XPS P2p, C1s, K2p, and O1s core-level spectra of bare CN and KPD-CN-7.5. (d) ^{31}P MAS NMR spectra of bare CN and KPD-CN-7.5.

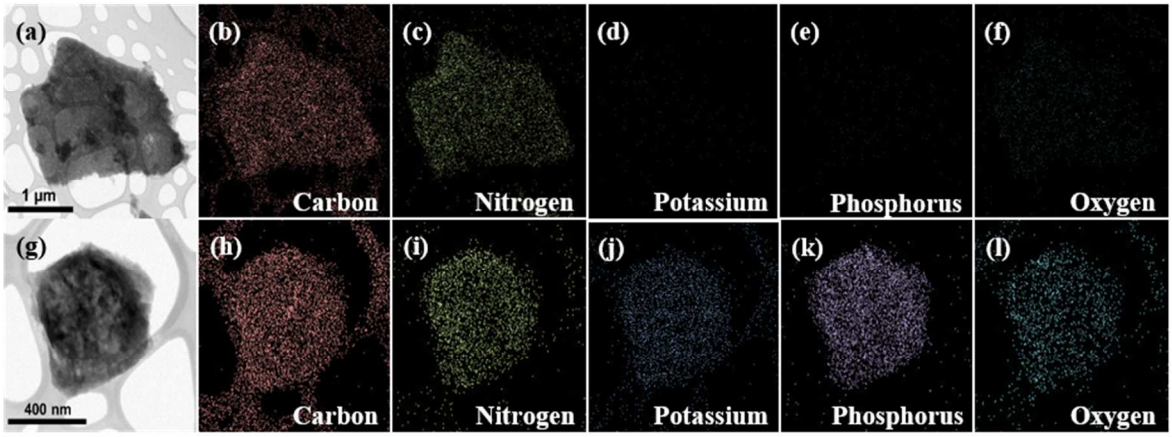

Figure 3. (a) TEM image of bare CN. (b-f) EDX mapping corresponding to panel (a). (g) TEM image of KPD-CN-7.5. (h-l) EDX mapping corresponding to panel (g). Red, green, blue, purple, and sky-blue color represent C (b and h), N (c and i), K (d and j), P (e and k), and O (f and l) elements, respectively.

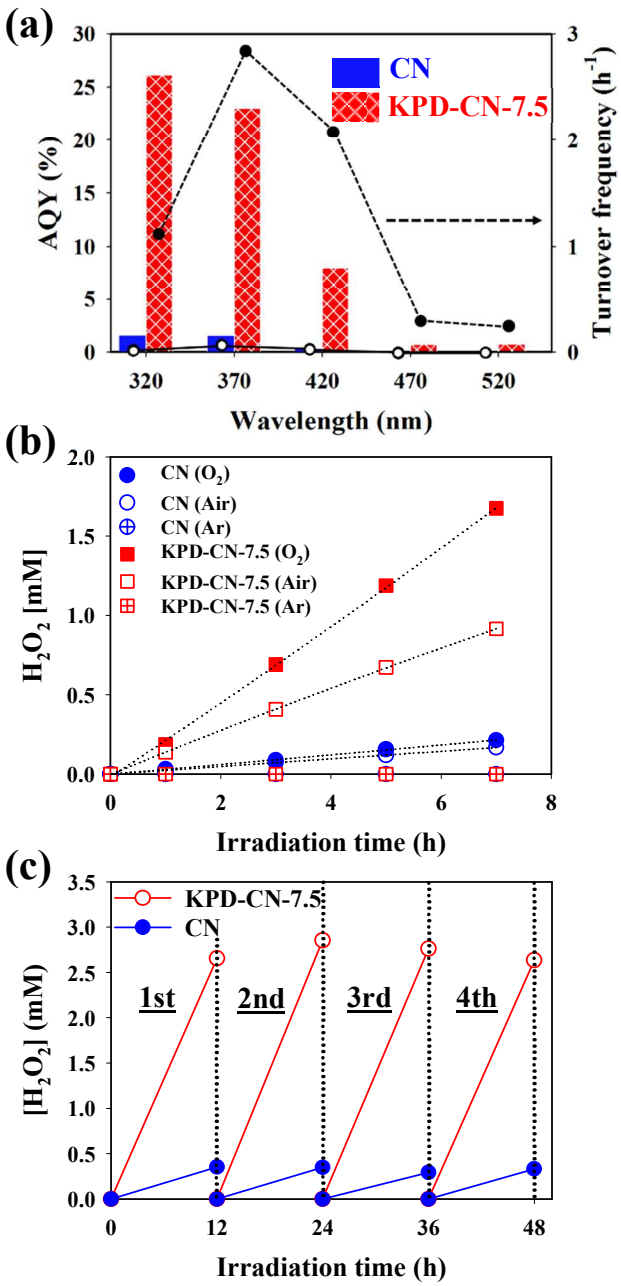

Figure 4. (a) Apparent quantum yield (AQY, Left axis) and turnover frequency (Right axis) of bare CN and KPD-CN-7.5 for H_2O_2 production under monochromatic light irradiation. (b) Comparison of the photoproduction of H_2O_2 under air-, N_2-, and O_2-saturated conditions for bare CN and KPD-CN-7.5. (c) Repeated runs of H_2O_2 generation in the

visible light-irradiated suspension of bare CN and KPD-CN-7.5. (b, c) The experimental conditions were: 0.5 g/L of photocatalyst, 10 vol% of ethanol, pHi = 3.0, and $\lambda \geq 420$ nm (polychromatic).

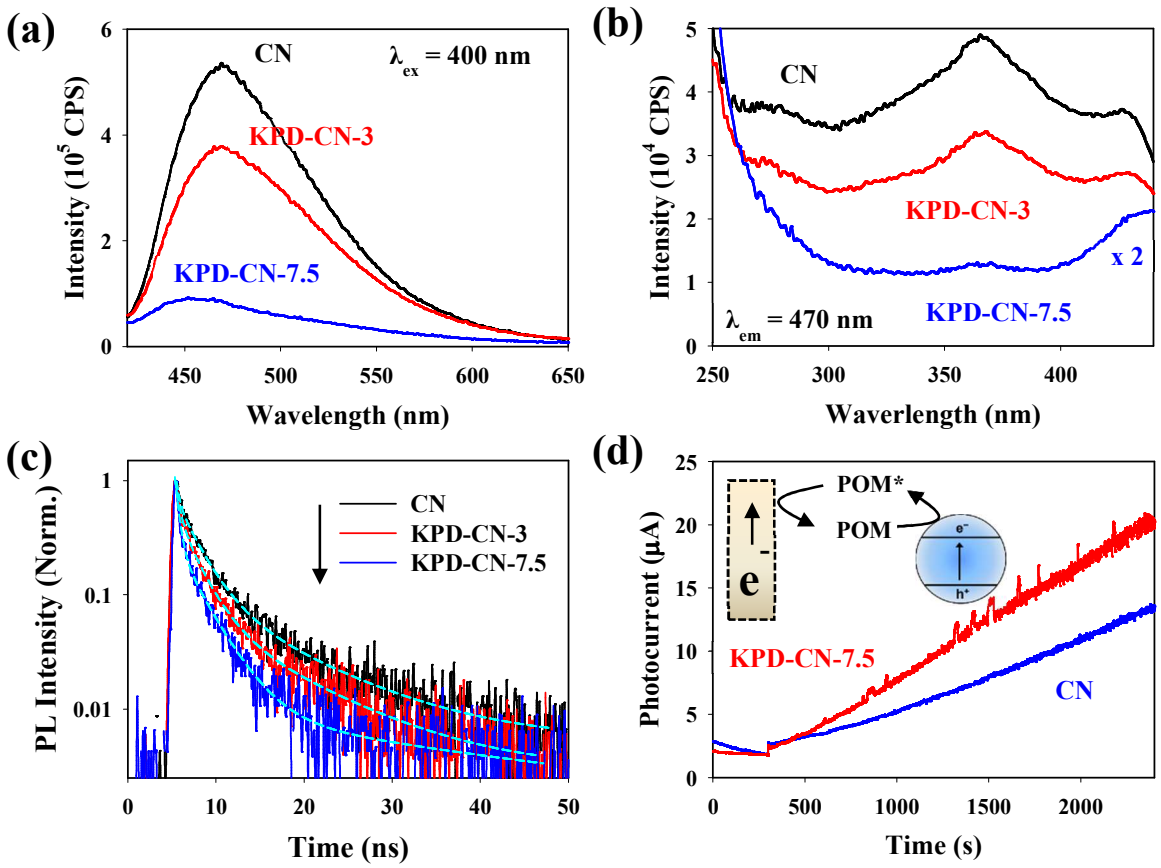

Figure 5. (a) PL emission spectra (λ_{ex} = 400 nm) and (b) PL excitation spectra at 470 nm of bare CN, KPD-CN-3, and KPD-CN-7.5. (c) TRPL spectra monitored at 480-490 nm of bare CN, KPD-CN-3, and KPD-CN-7.5 coated on glass slide after the excitation with 400 nm laser pulse. The curves were fitted to triexponential equation: $y = y_0 + A_1\exp(-t/\tau_1) + A_2\exp(-t/\tau_2) + A_3\exp(-t/\tau_3)$. (d) Time-profiles of POM-mediated photocurrent collected on a Pt electrode in the irradiated suspension of bare CN and KPD-CN-7.5. The experimental conditions were: 0.5 g/L catalyst, 2 mM $PW_{12}O_{30}^{3-}$, pH_i = 3, $\lambda \geq 420$ nm, 0.1 M $NaClO_4$, Pt electrode held at 0.7 V (vs Ag/AgCl), and continuously Ar-purged.

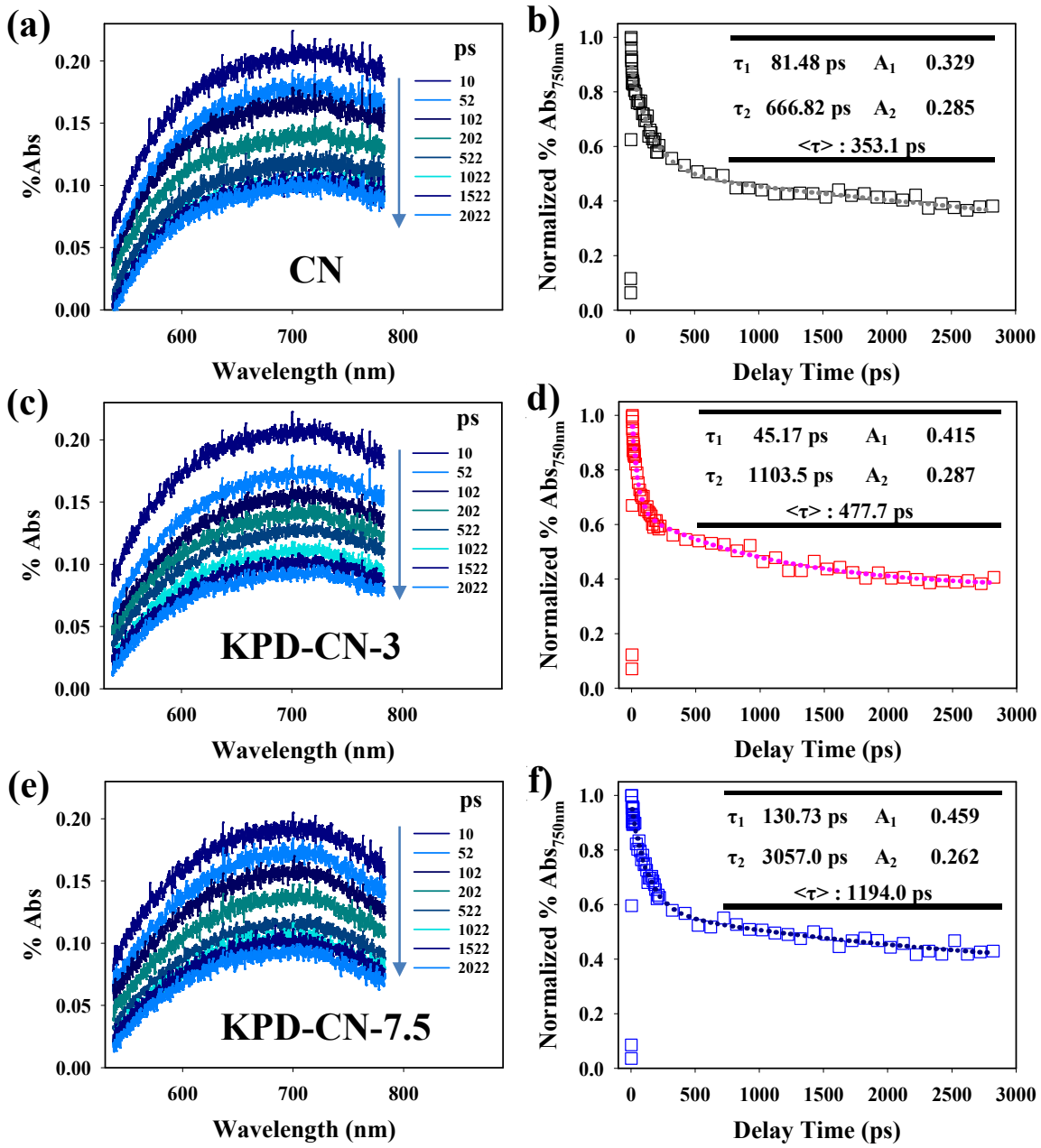

Figure 6. Time-resolved diffuse reflectance spectra for (a) bare CN, (c) KPD-CN-3, and (e) KPD-CN-7.5 recorded by 400 nm femtosecond laser pulse excitation under air. Decay curves of transient absorption intensity at 750 nm for (b) bare CN, (d) KPD-CN-3, and (f) KPD-CN-7.5. The dotted line curves are fitted to the biexponential equation: $y = y_0 + A_1\exp(-t/\tau_1) + A_2\exp(-t/\tau_2)$.

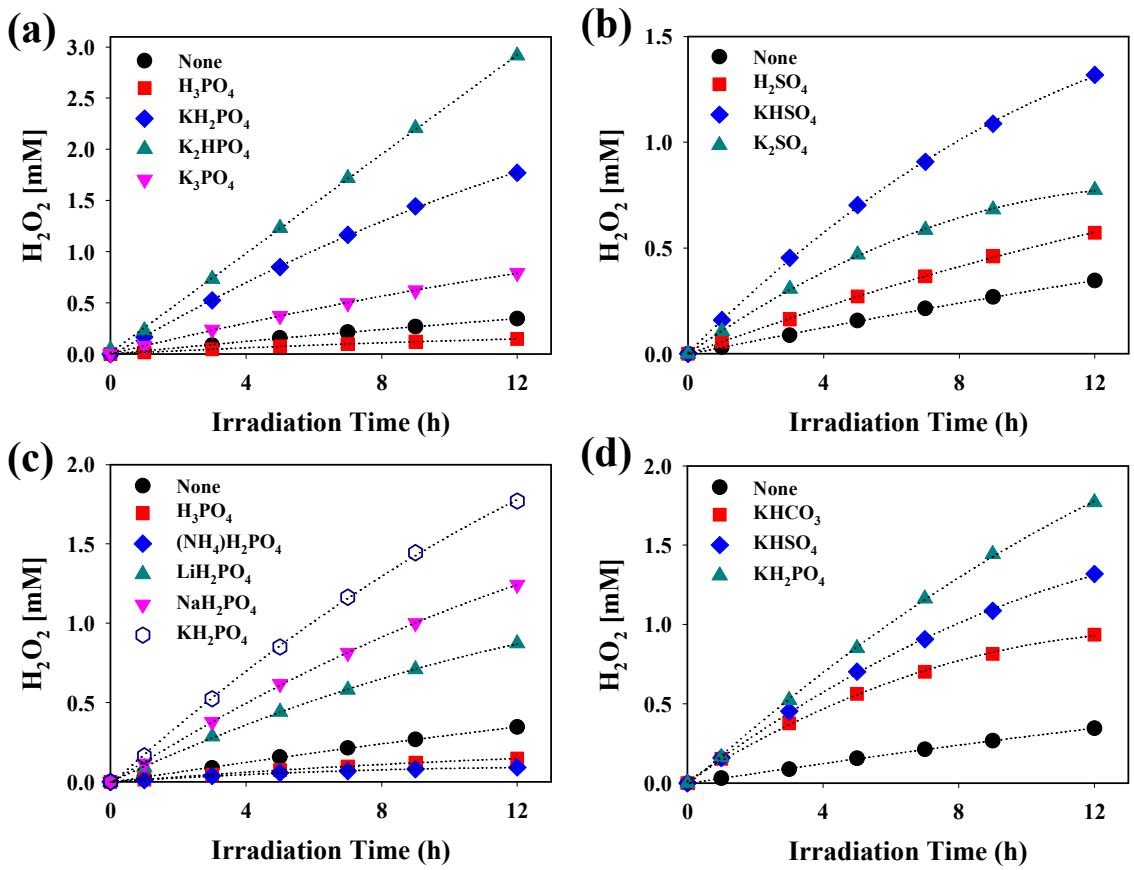

Figure 7. (a) Different types of potassium phosphate. (b) Different kinds of potassium sulfate. (c) Cationic effect based on dihydrogen phosphate species. (d) Anionic effect based on potassium. The experimental conditions were as follows: 0.5 g/L of photocatalyst, 10 vol.% of ethanol, pH_i = 3.0, and continuous O_2-purged atmosphere.

Table of content (TOC)